Molecular Dynamics Simulation of WSK-3, a Computationally Designed, Water-Soluble Variant of the Integral Membrane Protein KcsA

Jonathan Bronson, One-Sun Lee, and Jeffery G. Saven
Makineni Theoretical Laboratories, Department of Chemistry, University of Pennsylvania, Philadelphia, Pennsylvania 19104

ABSTRACT Poor solubility and low expression levels often make membrane proteins difficult to study. An alternative to the use of detergents to solubilize these aggregation-prone proteins is the partial redesign of the sequence so as to confer water solubility. Recently, computationally assisted membrane protein solubilization (CAMPS) has been reported, where exposed hydrophobic residues on a protein's surface are computationally redesigned. Herein, the structure and fluctuations of a designed, water-soluble variant of KcsA (WSK-3) were studied using molecular dynamics simulations. The root mean square deviation of the protein from its starting structure, where the backbone coordinates are those of KcsA, was 1.8 Å. The structure of salt bridges involved in structural specificity and solubility were examined. The preferred configuration of ions and water in the selectivity filter of WSK-3 was consistent with the reported preferences for KcsA. The structure of the selectivity filter was maintained, which is consistent with WSK-3 having an affinity for agitoxin2 comparable to that of wild-type KcsA. In contrast to KcsA, the central cavity's side chains were observed to reorient, allowing water diffusion through the side of the cavity wall. These simulations provide an atomistic analysis of the CAMPS strategy and its implications for further investigations of membrane proteins.

INTRODUCTION

Proteins in the cell membrane play a crucial role in many biological processes, such as endocytosis and cell signaling. A large fraction of known drugs are targeted toward membrane proteins or membrane protein linked receptors (1). Despite the difficulties of working with aggregation-prone membrane proteins, there have been striking recent successes in determining their structures, providing profound insight into their activity (2). Most structural studies of membrane proteins solubilize the protein using detergents or micellar systems, whereupon the proteins may be crystallized or studied using NMR methods. Nonetheless, membrane proteins remain difficult to study due to low levels of expression, low stability in detergent-solubilized forms, and reluctance to pack into diffraction quality crystals. To facilitate the study of membrane proteins, computational redesign of sequence has recently been applied (3,4).

A broadly applicable computationally assisted membrane protein solubilization strategy (CAMPS) was recently reported (4). Exposed hydrophobic residues are targeted for mutation, and a statistical mechanics based approach has been used to estimate the expected site-specific amino acid probabilities at these variable sites in a water-soluble protein with the same structure (5–7). The goal of CAMPS is to engineer one or more novel, water-soluble proteins that expresses in high yield but still maintain the essential structural and functionally related properties of the parent membrane protein.

One of the first proteins studied with this strategy was the potassium channel KcsA from the bacteria *Streptomyces lividans*. The potassium channel was chosen as a target for solubilization for two reasons (4). There are a number of high resolution structures of the membrane soluble form, which are useful for both structure based redesign of the protein and ultimately for comparison with the structures of designed, water-soluble variants (8,9). KcsA has been extensively studied biochemically and biophysically, providing a number of functionally related assays, which are useful in comparing the properties of KcsA and any designed, water-soluble analog.

Previous analysis of potassium channel sequences and structures has enabled researchers to explore the relation between sequence, structure, and physiological function (10). These channels play important roles in nerve and muscle excitation, hormonal secretion, cell proliferation, and maintenance of osmotic pressure as well as providing important medicinal targets (11). The selectivity of these channels for potassium ions is associated with a conserved sequence motif TXGYG (X is V in KcsA) located in the pore region (12). All potassium channels are thought to share a similar core structure, which was first revealed by x-ray crystallographic studies of KcsA (8). The general architecture of KcsA is outlined in Fig. 1. Four identical subunits, each comprising three α-helices, are dispersed symmetrically around a common axis central to the pore. Each subunit has two transmembrane (TM) helices and a pore loop between the two TMs. The pore loop comprises a descending pore helix and ascending filter region. The filter region contains potassium-binding sites formed by a ring of backbone oxygen atoms oriented toward the pore interior. There are four potassium-binding sites in the selectivity filter ($S_1 \sim S_4$), two

Submitted June 17, 2005, and accepted for publication October 21, 2005.

Address reprint requests to Jeffery G. Saven, Fax: 215-573-0980; E-mail: saven@sas.upenn.edu.

0006-3495/06/02/1156/08 $2.00

doi: 10.1529/biophysj.105.068965

at the filter's mouth (S_0, S_{ext}), and one in the center of the protein (S_{cavity}) (9) (see Fig. 1). In addition, the functionally important association of a scorpion toxin (agitoxin2) with a ''humanized'' sequence variant of KcsA has been well characterized (13).

High quality KcsA structures have allowed a number of groups to examine KcsA using molecular simulations. Free energy simulations investigating ion translocation through the filter found that a simple cycling is energetically most favorable between two alternate states ($S_1^{H_2O}S_2^{K^+}S_3^{H_2O}S_4^{K^+}$) and ($S_1^{K^+}S_2^{H_2O}S_3^{K^+}S_4^{H_2O}$), where the superscript is the molecule occupying the corresponding site (14). In molecular dynamics (MD) studies, the KcsA structure is stable over several nanoseconds of simulation. Root mean square deviations (RMSD) of the protein's backbone from the starting (experimental) crystal structure range from 1.6 to 2.5 Å (15,16). The most flexible part of the protein has been found to be the turret region. The selectivity filter is the most rigid, and the TM helices are intermediate, with the inner helix being more rigid than the outer helix (15,17–19). The concerted movement of water and ions through the filter has been observed in MD (15,17). The channel's central cavity has been observed to contain ~38 water molecules (17,18).

The water-soluble variant WSK-3 differs from KcsA by 33 mutations per subunit. The mutated residues are highlighted in red in Fig. 1, which shows that these residues are largely on the exterior of the structure. WSK-3 expresses well in *Escherichia coli* (4) and shares many properties with a ''humanized'' membrane-bound variant KcsA, including: a), a highly α-helical secondary structure, b), a tetrameric quaternary structure, c), specific binding to agitoxin2 with the same affinity as the membrane-bound form (13), and d), inhibition of the toxin binding by tetraethylammonium (4). Of course the solubilization of the protein precludes its most important functional property, selective ion conduction through the membrane. The goal of such redesign, however, is to obtain water-soluble variants of membrane proteins that retain structure and functionally related properties of the parent membrane protein. Indeed, properties such as selective toxin binding are likely to require a well-structured pore region. It is of great interest then to further explore the properties of WSK-3 at the atomistic level in light of what is known about KcsA.

In this work we investigate WSK-3 using MD simulations. The simulations provide a molecular perspective on the structure and fluctuations of WSK-3 in a solvated environment. The global structure of the protein and local structures of the selectivity filter and hydrophobic cavity are examined. Although many of the structural features of KcsA are retained, sites for water permeation into the channel that are unique to WSK-3 are also identified. The results have implications not only for better understanding WSK-3 but also for the solubilization and study of membrane proteins.

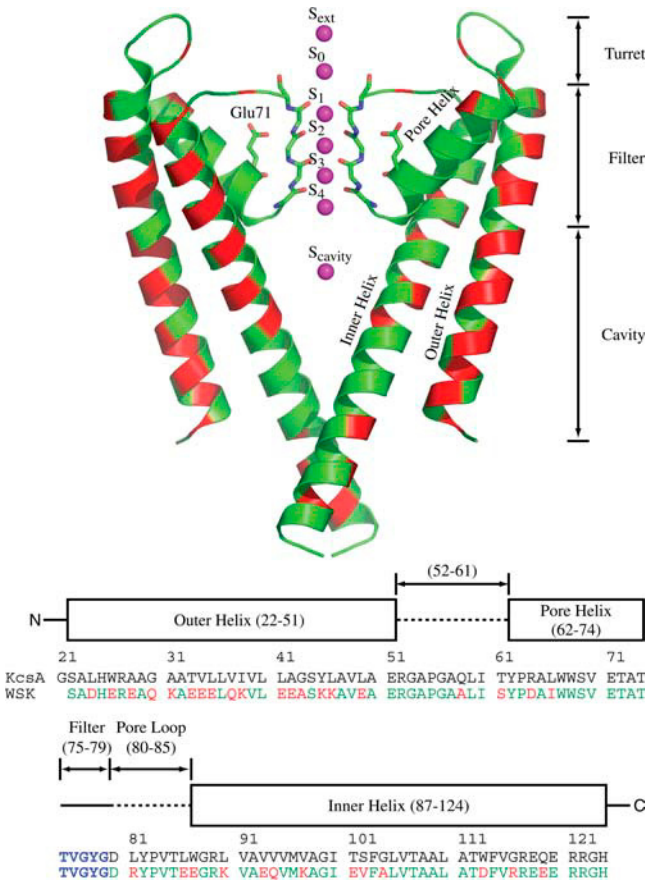

FIGURE 1 Structure of WSK-3 and its sequence. Mutated residues are shown in red, wild-type residues are shown in green. Sequences for KcsA and WSK-3 are shown for comparison (*red* designates mutations). The selectivity filter residues are highlighted in blue. All molecular images were rendered using PyMOL (38).

METHODS

Four different simulations of WSK-3 were performed (Table 1). Simulations 1, 3, and 4 used different initial configurations of potassium in the protein. Simulation 2 explored a different ionization state (neutral rather than ionized) for Glu^{71}. Multiple ion configurations were considered because the timescales required for ion diffusion through the channel, 10 ns or more in the presence of an applied voltage (20), are too long be observed in the simulation. Different starting positions of the ions were used to explore the stability of different ion configurations. We explored both ionization states of Glu^{71} because it plays an important structural role in the ion filter. It is

TABLE 1 Starting configuration of potassium atoms inside WSK-3 and the protonation state of Glu^{71}

	Run 1	Run 2	Run 3	Run 4
Site 0	H_2O	H_2O	H_2O	K^+
Site 1	H_2O	H_2O	K^+	H_2O
Site 2	K^+	K^+	H_2O	K^+
Site 3	H_2O	H_2O	K^+	H_2O
Site 4	K^+	K^+	H_2O	K^+
Cavity	H_2O	H_2O	K^+	H_2O
Glu^{71} protonation	Yes	No	Yes	Yes

protonated in membrane-soluble KcsA and forms a hydrogen bond with Asp^{80} (21). Glu^{71} is less likely to be protonated in WSK-3, however, since the protein is surrounded by a more hydrophilic environment.

The backbone coordinates of the high resolution crystal structure of KcsA (Protein Data Bank accession code: 1k4c) were used as the starting point for the simulations (9). This is the same template crystal structure that was used to design WSK-3 (4). The atomic positions of the backbone and side chains common to both proteins were those of the crystal structure. The side chains unique to WSK-3 were placed in their most probable rotamer conformation, as determined by the computational sequence design (4).

The protein was placed in a 71.4 Å × 71.4 Å × 80.9 Å water box using the SOLVATE (22) module as implemented in VMD (23). The modified TIP3P model (24,25) was used for water molecules. Potassium and chloride ions were added to the water box to make the system charge neutral and mimic a 150 mM KCl concentration. This required the placement of 25–28 K^+ and 2–4 Cl^- in each water box, depending on the simulation. (Repeated simulations found the results presented herein are insensitive to the initial configuration of these ions.) Potassium ions were placed in the selectivity filter and central cavity using the coordinates from the 1k4c structure. Vacant spaces in the selectivity filter were filled with water. Twenty crystallographic water molecules, four beside Glu^{71} and 16 in the cavity, were used in the simulation. Twenty-two additional water molecules were placed in the cavity, consistent with the 38 observed in previous KcsA simulations (17,18,26). Each system had a total of ~38,000 atoms.

All simulations were performed using NAMD (27) with the CHARMM22 force field (24). The simulations began with a 1000 step minimization of the designed side chains and solvent to remove any bad contacts. The protein backbone, unmutated side chains, and crystallographic water and potassium were fixed for this minimization. Then a 3000 step energy minimization was performed with just the backbone atoms of WSK-3 fixed, followed by a 3500-step energy minimization of all the atoms. The backbone atoms were harmonically constrained with a restraining constant of 10.0 kcal/mol/$Å^2$, and the systems were heated to 300 K over the course of 6 ps at constant volume. The simulations were equilibrated for 500 ps with NPT ensemble (1 atm, 300 K) while the harmonic constraints were gradually turned off. With no harmonic constraints, the simulations ran for 3 ns in the NPT ensemble using Langevin dynamics at a temperature of 300 K with a damping coefficient of $\gamma = 5\ ps^{-1}$. Pressure was maintained at 1 atm using the Langevin piston method with a piston period of 100 fs, a damping time constant of 50 fs, and a piston temperature of 300 K (28,29). Nonbonded interactions were smoothly switched off from 10 to 12 Å. The list of nonbonded interactions was truncated at 14 Å. Covalent bonds involving hydrogen were held rigid using the SHAKE algorithm, allowing a 2 fs time step. Periodic boundary conditions were used, and electrostatic interactions were computed using the particle mesh Ewald summation with 1 Å grid width (30). Atomic coordinates were saved every 1 ps for the trajectory analysis during the last 2 ns of MD simulation.

RESULTS AND DISCUSSION

Global structure of WSK-3

Despite the differences in sequence and solvent environment, WSK-3 maintained all the secondary, tertiary, and quaternary structures of KcsA throughout all four simulations. As with KcsA, WSK-3 maintains a tetrameric structure whose primary structural elements are an inner helix, an outer helix, a pore helix, and a selectivity filter. The RMSD of the protein's backbone atoms relative to its starting configuration (the backbone coordinates of which are those of the KcsA crystal structure) are listed in Table 2. The RMSD values for previous KcsA simulations are included for reference as well. It should be noted that the RMSD values of the KcsA simulations are comparable to or greater than the RMSD values observed in the WSK-3 simulations. Thus, the designed, water-soluble analog of the potassium channel does not deviate from the crystal structure of KcsA any more than KcsA does in simulations of the membrane-bound protein (15–18).

TABLE 2 RMSD of the backbone of WSK-3 relative to its starting structure (the coordinates contained in 1k4c)

WSK-3 simulations	RMSD (Å)
Run 1	1.79 ± 0.18
Run 2	1.87 ± 0.16
Run 3	1.64 ± 0.09
Run 4	1.98 ± 0.20
Published KcsA simulations	
(18)*	2.3 ± 0.1
(17)†	1.9
(16)*	~2.5
(15)†	1.6
(15)‡	2.0

*Backbone atoms.
†α-carbons only.
‡All atoms.
RMSD values of previous simulation studies of KcsA are shown for comparison.

To examine the flexibility of the different regions of the protein, the root mean square fluctuations (RMSF) of individual backbone atoms about their average positions were calculated. These values are listed in Table 3. The area around the selectivity filter was the most rigid, and the turret region was the most flexible. The inner helix was more rigid than the outer helix. Similar features have also been observed in previous simulations of KcsA (15,17–19).

Salt bridges

The most pronounced difference between WSK-3 and KcsA is the presence of large numbers of hydrophilic and ionizable side chains on the exterior of the structure. As a result, complementary interactions between charged residues appear in the WSK-3 structure that results from the statistical, computationally assisted design calculations (SCADS), calculations which do not consider solvent explicitly (4). To analyze the salt bridge interactions in WSK-3 in solution, the occupation of potential salt bridge interactions was

TABLE 3 RMSF of WSK-3's backbone atoms about their average position (in Å)

	Residue No.	Run 1	Run 2	Run 3	Run 4
Pore helix	62–74	0.52	0.49	0.53	0.55
Selectivity filter	75–79	0.53	0.48	0.62	0.51
Pore loop	80–86	0.67	0.62	0.64	0.59
Inner helix	87–124	0.69	0.65	0.66	0.63
Outer helix	22–51	0.80	0.78	0.73	0.79
Turret	52–61	1.29	1.21	1.17	1.30

The values shown are averaged over all the backbone atoms in each region.

estimated as the fraction of configurations where the two charged residues were within 3.7 Å of each other, measured as the minimum, interresidue N-O distance involving the two side chains (31). The occupancies were averaged over the four subunits for each run, but the four runs were analyzed separately. The results of this analysis are summarized in Table 4.

Most of WSK-3's salt bridges are clustered on the outer helix, the C-terminal end of the inner helix (after residue 116), or near the selectivity filter. Almost all of the salt bridges involve at least one engineered residue. Intrasubunit salt bridges occur at the outer helix and the C-terminal end of the inner helix. The most prominent of these are K^{38}–E^{35}, R^{117}–D^{113}, and R^{121}–E^{118}. As expected for a helical protein, these interactions tend to involve $(i, i + 3)$ or $(i, i + 4)$ interactions between residues and likely play a role in stabilizing WSK-3's secondary structure. Intersubunit salt bridges form between basic residues near the C-terminus and acidic residues near either the N-terminus (R^{117}–D^{24}) or at the C-terminus (R^{116}–E^{118} and R^{122}–E^{119}). These bridges likely help maintain the quaternary structure of the protein. Interestingly, the designed L116R mutation was found to be important for reducing the population of high molecular weight aggregates (4).

The important salt bridge between Asp^{80} and Arg^{89} found in KcsA is conspicuously absent from the WSK-3 simulations. It appears to have been replaced by a salt bridge between Arg^{89} and the engineered residue Asp^{64}. Asp^{80} and Arg^{89} still maintain an average distance of 5.1 ± 0.6 Å during the simulations (as measured by the nucleus to nucleus distance of the closest nitrogen/oxygen pair). A water molecule occupies the space between the two and forms hydrogen bonds to both residues.

TABLE 4 Salt bridges formed during MD simulations

Base	Acid	Chain	Engineered residues	Run 1 (%)	Run 2 (%)	Run 3 (%)	Run 4 (%)
Arg^{27}	Asp^{24}	Intra	Asp^{24}	27.6	51.9	47.8	59.2
Lys^{31}	Glu^{28}	Intra	Glu^{28}	72.8	50.7	30.6	47.6
Lys^{38}	Glu^{35}	Intra	Both	84.3	66.4	64.5	73.2
Lys^{45}	Glu^{49}	Intra	Both	30.9	51.7	70.6	35.4
Glu^{71}	Asp^{80}	Intra	Neither	98.5	N/A	86.1	99.4
Arg^{81}	Asp^{64}	Intra	Both	57.9	62.7	81.0	84.0
Arg^{81}	Asp^{80}	Intra	Arg^{81}	0.0	79.3	0.0	3.1
Arg^{89}	Asp^{64}	Inter	Asp^{64}	83.3	99.9	89.1	70.3
Arg^{89}	Asp^{80}	Inter	Neither	0.2	1.5	0.3	27.8
Arg^{116}	Asp^{113}	Intra	Both	28.9	76.0	43.0	58.2
Arg^{116}	Glu^{118}	Inter	Arg^{116}	95.0	74.5	99.7	89.2
Arg^{117}	Asp^{24}	Inter	Asp^{24}	55.6	41.9	78.1	29.4
Arg^{117}	Asp^{113}	Intra	Asp^{113}	97.5	100.0	99.1	99.8
Arg^{121}	Glu^{118}	Intra	Neither	75.1	100.0	100.0	100.0
Arg^{122}	Glu^{119}	Inter	Glu^{119}	49.8	21.7	86.9	49.2

The participating residues, whether they were engineered in designing WSK-3, and the occupancy (percentage time partners are within 3.7 Å of each other) are listed. Salt bridges that form at least ~50% of the time on average, that depend on the ionization state of Glu^{71} (R^{81}–D^{80}) or that were found to be important in KcsA (R^{89}–D^{80}) are shown.

Effect of Glu^{71} ionization

From the early structures of KcsA, the protonation state of Glu^{71} was unclear (8). In the absence of structural considerations the residue was expected to be deprotonated at neutral pH, and several simulations were performed under that assumption (16,18). Free energy simulations and Poisson-Boltzmann calculations using the KcsA structure, however, have suggested that the residue's pKa is 13.6, and as a result it should be protonated (21). This prediction is consistent with a high resolution crystal structure of KcsA (9).

The residue's protonation state is nontrivial since it may play an important role in the function of the wild-type protein. Continuum electrostatic calculations involving KcsA indicate that the free energy of potassium ions at S_1 is further stabilized by at least 6 kcal/mol when the Glu^{71} is deprotonated (32). Unfortunately, the ionization state of Glu^{71} in WSK-3 is unknown, although it may well be ionized due to the exposure to water rather than lipid. We performed simulations comparing both ionization states (simulations Run 1 and Run 2).

The simulations of WSK-3 show that the ionization state of Glu^{71} affects the position of several residues near the selectivity filter. When Glu^{71} is protonated, it forms a hydrogen bond with Asp^{80}, just as in KcsA. When Glu^{71} is deprotonated this hydrogen bond cannot form, so Asp^{80} rotates away from Glu^{71} and forms a salt bridge with Arg^{81} (the result of an engineered L81R mutation). This, in turn, pulls Arg^{81} away from Asp^{64}, allowing Asp^{64} to form a shorter bond with Arg^{89}. These conformational changes are reflected in the average distances of these residues from Asp^{80}, shown in Fig. 2. The average distance between Asp^{80}–Glu^{71} is 2.73 ± 0.19 Å

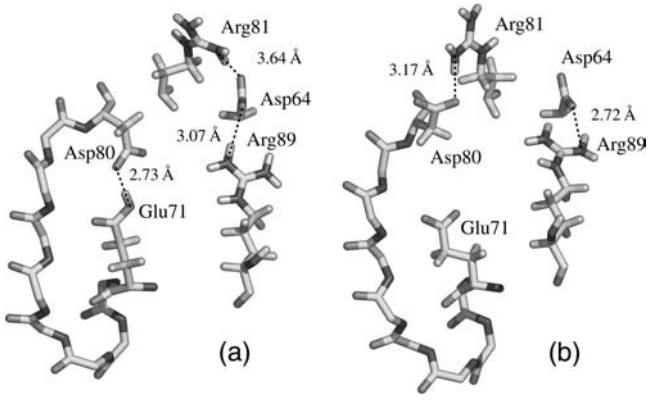

FIGURE 2 Effects of Glu^{71} ionization on the region surrounding the selectivity filter. The backbone of the selectivity filter and side chains of important nearby residues are shown from Run 1 (*a*) and Run 2 (*b*) after 3 ns of simulation. Average hydrogen bond lengths for key residues are shown (measured from the oxygen atom of the acid to the nitrogen atom of the base). When Glu^{71} is protonated, it forms a hydrogen bond with Asp^{80}. The hydrogen bond between Arg^{89} and Asp^{80} found in KcsA is replaced by one between Arg^{89} and Asp^{64}. Asp^{64} hydrogen bonds to Arg^{81} as well. Deprotonation of Glu^{71} causes Asp^{80} to rotate away from it and hydrogen bond with Arg^{81}, pulling Arg^{81} away from Asp^{64}.

when Glu^{71} is protonated (Run 1), and it is increased to 7.14 ± 0.56 Å when Glu^{71} is in its deprotontated state (Run 2). In contrast, the average distance between Asp^{80}–Arg^{81} is 6.27 ± 0.59 Å in Run 1 and it decreases to 3.17 ± 0.73 Å in Run 2.

The behavior of the four crystallographic water molecules near the selectivity filter also depends on the ionization state of Glu^{71}. When Glu^{71} is protonated, the water molecules have a clear structural role in the selectivity filter; they remain near the backbone nitrogens of Tyr^{78}, Gly^{79}, and Asp^{80} and are held in place by polar interactions with the surrounding protein. The water molecules are partially solvent exposed and hydrogen bond with the bulk solvent 60% of the time. Movement of Asp^{80} away from the deprotonated Glu^{71} in Run 2 makes the backbone of the selectivity filter more solvent accessible. This allows the crystallographic water to exchange with the solvent easily. Two or three solvent water molecules occupy the space that was initially occupied by Asp^{80} and the crystallographic water.

Cavity and water flow

The greatest differences between the simulations of KcsA and WSK-3 occur in the central cavity. Unlike KcsA, the walls of the cavity of WSK-3 allow water to diffuse in and out through its sides. Movement of the large nonpolar residues that line the cavity's walls (Ile^{100} and Phe^{103}) appears to be responsible for this. The side chains of these residues were observed to rotate into and out of the cavity during the simulations. Depending on the extent of the side-chain collapse, individual water molecules or hydrogen-bonded chains of water flow in and out of the cavity, as illustrated in Fig. 3. These side-chain motions may be a result of WSK-3′s aqueous environment: the position of these side chains is no longer stabilized through hydrophobic interactions with the phospholipid bilayer so there is a smaller energetic penalty for them to move into the cavity.

The number of water molecules in the cavity varied during the simulations but was typically between 24 and 34. The fluctuation of water inside the cavity of Runs 1 and 2 is shown in Fig. 4. The number was greater during the Glu^{71} deprotonated run (32.9 ± 1.7 in Run 2) than the Glu^{71} protonated run (26.1 ± 2.4 in Run 1) but was still short of the 38 water molecules reported in most simulations of KcsA. Fluctuations in the amount of water in the cavity also appear to be a result of the previously discussed side-chain motions; when the side chains collapse into the cavity it decreases the number of water molecules inside, and when the side chains return to their original position the number of water molecules inside the cavity increases.

Water permeation through the cavity walls is the largest difference between the simulations of KcsA and WSK-3. Water diffusion is much less likely to take place through the sides of KcsA's cavity, since it is in the phospholipid bilayer. Mutations to the cavity walls, such as T100E and S101V, may have contributed to the cavity's water permeability as well. These simulations suggest that the design of WSK-3 could be improved for this part of the protein to better mimic the structure of KcsA.

The selectivity filter

In this study we explored two configurations of potassium ions in the selectivity filter. In the first, the 1,3 configuration, ions occupy the S_1 and S_3 sites and water occupies the S_2 and S_4 sites (9). In the second, the 2,4 configuration, ions occupy the S_2 and S_4 sites and water occupies the S_1 and S_3 sites (see Fig. 1). Ions are thought to move through KcsA by alternating between these two configurations (14,33–35). In addition, we examined WSK-3′s ability to restrain a potassium ion in its cavity in Run 3 and we explored the S_0 site in Run 4.

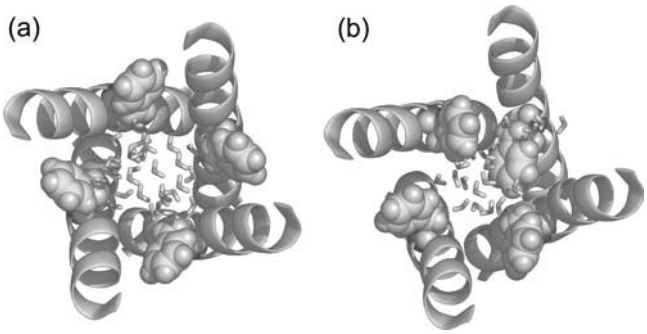

FIGURE 3 Snapshots of diffusing water through the cavity wall. The side chains of Phe^{103} and water molecules are shown using space filling/stick representation. The top half of the protein and all other side chains were removed for clarity. (*a*) The starting structure of WSK-3. (*b*) During the MD simulation, the Phe^{103} and Ile^{100} (not shown for clarity) periodically drift into the cavity, making pores that water can diffuse through. The water can form a hydrogen-bonded chain as it diffuses through the cavity.

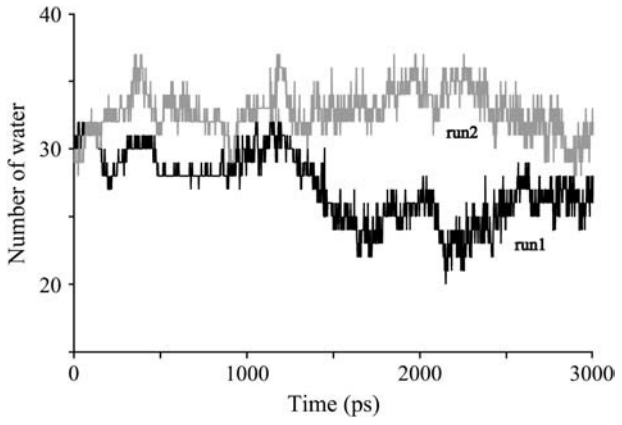

FIGURE 4 The number of water molecules inside the cavity of WSK-3 as a function of time. The mean value and standard deviation (1σ) is 26.1 ± 2.4 Å in Run 1, and 32.9 ± 1.7 Å in Run 2.

To quantify the features of the ions in the selectivity filter, we looked at the vertical distance of the ions from the protein's center of mass for each run. The 2,4 ion configuration is extremely stable in WSK-3. The ions in Runs 1 and 2 showed very little movement throughout the simulations. During Run 3, however, the ions in the 1,3 configuration moved to the 2,4 configuration after 500 ps. This transition is shown in Fig. 5. The transition takes ~150 ps and involves the concerted movement of water molecules and ions. First the S_1 ion shifts down to the S_2 site. This movement forces the water at the S_2 site into the side of the filter, between the S_2 and S_3 sites. Then the ion at S_3 moves down to the S_4 site and the sandwiched water moves into the S_2 site completing the transition. The same transition of ions from the 1,3 configuration to the 2,4 configuration has been observed in simulations of KcsA (15). The ions were stable for 500 ps of Run 3 before transitioning to the 2,4 configuration, suggesting that WSK-3 can bind potassium in the 1,3 configuration but that the 2,4 may be preferred. The same is thought to be true in KcsA, where free energy perturbation calculations show that the 2,4 configuration is the lowest energy arrangement of ions and water in the filter and the 1,3 configuration is the second lowest energy arrangement (14).

S_0 and S_{ext} sites and inhibitor binding

In addition to the S_1–S_4 sites, there is a solvent-exposed binding site in KcsA called the S_0 site and a region of high potassium affinity directly above that called the S_{ext} site (see Fig. 1). Binding at both of these sites has been observed crystallographically and in MD simulations (9,36). The presence of the S_0 and S_{ext} sites in WSK-3, however, appears to depend on the ionization state of Glu^{71}. In Run 2, where Glu^{71} is deprotonated, an ion moves into the S_0 site within 750 ps of MD and remains there for the remaining 2250 ps of simulation. In addition, another ion is present at or near the S_{ext} site for over 85% of the last 2 ns of simulation.

No S_0 binding was observed in any of the three Glu^{71} protonated simulations. Moreover, the ion which started in the S_0 site during Run 4 leaves the selectivity filter as soon as the harmonic constraints are removed. The S_{ext} region still attracts ions during Runs 1 and 4, but only with 35% occupancy. The differences in ion binding are highlighted in Fig. 6. No ions entered the S_{ext} region during Run 3, possibly due to the additional electrostatic repulsion provided by the ion in the cavity.

Basis for inhibitor binding

Experimentally, agitoxin2 and tetraethylammonium cation, which bind to a modified form of KcsA (13), also selectively bind WSK-3 (4). Although these simulations do not provide quantitative estimates of ligand-protein binding affinities, the simulations do qualitatively inform WSK-3′s binding behavior. WSK-3′s selectivity filter and the region immediately surrounding it, which contain the key residues for ligand binding, maintain the local structure present in KcsA's crystal structure. The RMSD of this region is low, 0.9 Å, and

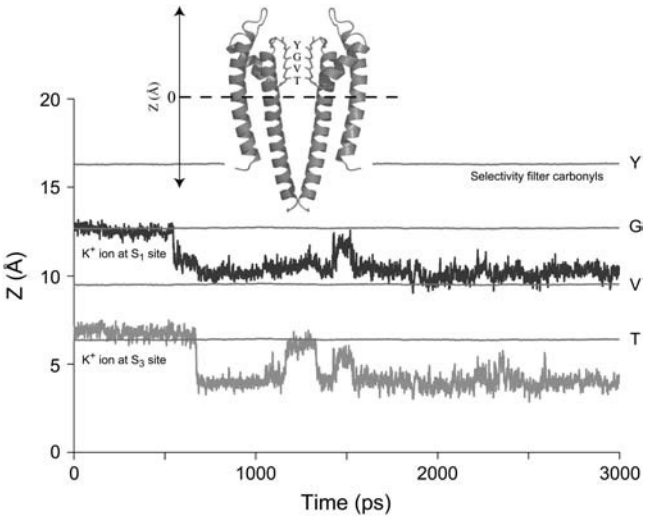

FIGURE 5 Displacement of filter ions along the channel axis during Run 3. Potassium ions at S_1 and S_3 transition to S_2 and S_4 after 500 ps of MD, where they remain for the rest of the simulation. Ions in the selectivity filter do not leave their positions in simulations that begin in the 2,4 configuration (not shown), suggesting an energetic preference for the 2,4 configuration over the 1,3 configuration. The positions of the carbonyl backbone oxygens of residues 75–79 are shown for reference.

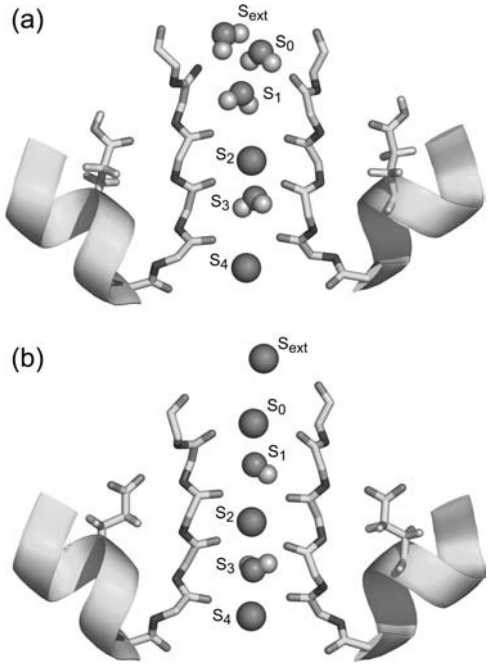

FIGURE 6 The position of potassium ions (*spheres*) and water molecules inside the selectivity filter. (*a*) Protonation of Glu^{71} prevents potassium from occupying S_0 and S_{ext} during the MD simulation (image from Run 1, 3 ns). (*b*) When Glu^{71} is deprotonated, however, S_0 and S_{ext} are occupied by potassium ions (image from Run 2, 3 ns).

none of these residues was mutated to create WSK-3. Given that the same residues exhibit similar structures and K^+ binding, it is not surprising that they also exhibit the same binding behavior for agitoxin2. Recent modeling results suggest that the ammonium group of a lysine residue on agitoxin2 threads into the selectivity filter (37). The structural conservation of this part of the channel in KcsA and WSK-3 is consistent with their similar binding selectivities and affinities.

CONCLUSIONS

In these simulations we have explored many of the structural and functionally related aspects of WSK-3. In particular, WSK-3 possesses many of KcsA's structural elements. The selectivity filter stably coordinates potassium ions and, like KcsA, the 2,4 ion configuration appears more stable than the 1,3. The RMSD (~1.8 Å) of the backbone atoms of WSK-3 (relative to the crystal structure of KcsA) is comparable to that observed in simulations of KcsA. Several differences were also observed, however. The most notable were the large movements of the cavity side chains and the cavity's reduced water capacity.

These simulation studies further inform efforts to solubilize membrane proteins using redesign of sequence. These results are consistent with previous experimental results (4), which together suggest that a protein can be redesigned so as to be taken out of the lipid bilayer and made soluble in water with high structural fidelity. However, nonpolar side chains may lose some structural rigidity in the absence of stabilizing hydrophobic interactions with the lipid membrane, as is observed for the Phe side chains that line the central cavity. In addition, the protonation state of residues may change as the local environment changes, but such changes in protonation states may actually help maintain desired characteristics of the protein, as observed for the occupancy of the S_0 and S_{ext} sites when Glu^{71} is deprotonated.

In conclusion, the overall similarity of WSK-3 to KcsA, especially in the region of the selectivity filter, suggests that WSK-3 retains many of the structural and functionally related properties of KcsA and may be of use in binding assays or drug discovery studies. It is important to note that these simulations do not address motions occurring on long timescales (more than 10 ns), such as opening and closing of the pore. Nonetheless, these simulations support the utility of CAMPS for arriving at soluble variants of membrane proteins. Additionally, such simulations can augment both computational design and experimental studies of water-soluble variants of membrane proteins. The molecular detail provided can be used to suggest further refinements to the designed sequences.

NAMD was developed by the Theoretical and Computational Biophysics Group in the Beckman Institute at the University of Illinois, Urbana-Champaign.

The authors gratefully acknowledge support from the National Institutes of Health (GM 61267) and the National Science Foundation (DMR 00-79909, CHE 99-84752). Computational resources were supported in part by National Science Foundation CHE 01-31132. J.G.S. is a Cottrell Scholar of Research Corporation.

REFERENCES

1. Drews, J. 2000. Drug discovery: a historical perspective. *Science*. 287: 1960–1964.
2. MacKinnon, R. 2004. Potassium channels and the atomic basis of selective ion conduction (Nobel lecture). *Angew. Chem. Int. Ed. Engl.* 43:4265–4277.
3. Slovic, A. M., C. M. Summa, J. D. Lear, and W. F. DeGrado. 2003. Computational design of a water-soluble analog of phospholamban. *Protein Sci.* 12:337–348.
4. Slovic, A. M., H. Kono, J. D. Lear, J. G. Saven, and W. F. DeGrado. 2004. Computational design of water-soluble analogues of the potassium channel KcsA. *Proc. Natl. Acad. Sci. USA*. 101:1828–1833.
5. Saven, J. G., and P. G. Wolynes. 1997. Statistical mechanics of the combinatorial synthesis and analysis of folding macromolecules. *J. Phys. Chem. B*. 101:8375–8389.
6. Zou, J. M., and J. G. Saven. 2000. Statistical theory of combinatorial libraries of folding proteins: energetic discrimination of a target structure. *J. Mol. Biol.* 296:281–294.
7. Kono, H., and J. G. Saven. 2001. Statistical theory for protein combinatorial libraries. Packing interactions, backbone flexibility, and the sequence variability of a main-chain structure. *J. Mol. Biol.* 306: 607–628.
8. Doyle, D. A., J. M. Cabral, R. A. Pfuetzner, A. L. Kuo, J. M. Gulbis, S. L. Cohen, B. T. Chait, and R. MacKinnon. 1998. The structure of the potassium channel: molecular basis of K+ conduction and selectivity. *Science*. 280:69–77.
9. Zhou, Y. F., J. H. Morais-Cabral, A. Kaufman, and R. MacKinnon. 2001. Chemistry of ion coordination and hydration revealed by a K+ channel-Fab complex at 2.0 angstrom resolution. *Nature*. 414:43–48.
10. Miller, C. 1988. Competition for block of a Ca-2+-activated K+ channel by charybdotoxin and tetraethylammonium. *Neuron*. 1:1003–1006.
11. Cook, N. S., editor. 1990. Potassium Channels: Structure, Classification, Function, and Therapeutic Potential. Halsted Press, New York.
12. Trauner, D. 2003. Potassium channels: symmetric, selective, and sensitive. *Angew. Chem. Int. Ed. Engl.* 42:5671–5675.
13. MacKinnon, R., S. L. Cohen, A. L. Kuo, A. Lee, and B. T. Chait. 1998. Structural conservation in prokaryotic and eukaryotic potassium channels. *Science*. 280:106–109.
14. Aqvist, J., and V. Luzhkov. 2000. Ion permeation mechanism of the potassium channel. *Nature*. 404:881–884.
15. Domene, C., and M. S. P. Sansom. 2003. Potassium channel, ions, and water: simulation studies based on the high resolution x-ray structure of KcsA. *Biophys. J.* 85:2787–2800.
16. Shrivastava, I. H., and M. S. P. Sansom. 2000. Simulations of ion permeation through a potassium channel: molecular dynamics of KcsA in a phospholipid bilayer. *Biophys. J.* 78:557–570.
17. Berneche, S., and B. Roux. 2000. Molecular dynamics of the KcsA K+ channel in a bilayer membrane. *Biophys. J.* 78:2900–2917.
18. Guidoni, L., V. Torre, and P. Carloni. 1999. Potassium and sodium binding to the outer mouth of the K+ channel. *Biochemistry*. 38:8599–8604.
19. Shrivastava, I. H., and M. S. P. Sansom. 2002. Molecular dynamics simulations and KcsA channel gating. *Eur. Biophys. J.* 31:207–216.
20. Bek, S., and E. Jakobsson. 1994. Brownian dynamics study of a multiply occupied cation channel—application to understanding permeation in potassium channels. *Biophys. J.* 66:1028–1038.

21. Berneche, S., and B. Roux. 2002. The ionization state and the conformation of Glu-71 in the KcsA K+ channel. *Biophys. J.* 82:772–780.

22. Grubmuller, H. 1996. SOLVATE. Version 1.2. Theoretical Biophysics Group, Institute for Medical Optics, Ludwig-Maximilians University, Munich.

23. Humphrey, W., A. Dalke, and K. Schulten. 1996. VMD: visual molecular dynamics. *J. Mol. Graph.* 14:33–38.

24. MacKerell, A. D., D. Bashford, M. Bellott, R. L. Dunbrack, J. D. Evanseck, M. J. Field, S. Fischer, J. Gao, H. Guo, S. Ha, D. Joseph-McCarthy, L. Kuchnir, et al. 1998. All-atom empirical potential for molecular modeling and dynamics studies of proteins. *J. Phys. Chem. B.* 102:3586–3616.

25. Jorgensen, W. L., J. Chandrasekhar, and J. D. Madura. 1983. Comparison of simple potential functions for simulating liquid water. *J. Chem. Phys.* 79:926–935.

26. Compoint, M., P. Carloni, C. Ramseyer, and C. Girardet. 2004. Molecular dynamics study of the KcsA channel at 2.0-angstrom resolution: stability and concerted motions within the pore. *Biochim. Biophys. Acta.* 1661:26–39.

27. Kale, L., R. Skeel, M. Bhandarkar, R. Brunner, A. Gursoy, N. Krawetz, J. Phillips, A. Shinozaki, K. Varadarajan, and K. Schulten. 1999. NAMD2: greater scalability for parallel molecular dynamics. *J. Comput. Phys.* 151:283–312.

28. Feller, S. E., Y. H. Zhang, R. W. Pastor, and B. R. Brooks. 1995. Constant-pressure molecular-dynamics simulation—the Langevin piston method. *J. Chem. Phys.* 103:4613–4621.

29. Martyna, G. J., D. J. Tobias, and M. L. Klein. 1994. Constant-pressure molecular-dynamics algorithms. *J. Chem. Phys.* 101:4177–4189.

30. Darden, T., D. York, and L. Pedersen. 1993. Particle mesh Ewald—an N.Log(N) method for Ewald sums in large systems. *J. Chem. Phys.* 98: 10089–10092.

31. Stickle, D. F., L. G. Presta, K. A. Dill, and G. D. Rose. 1992. Hydrogen-bonding in globular-proteins. *J. Mol. Biol.* 226:1143–1159.

32. Roux, B., S. Berneche, and W. Im. 2000. Ion channels, permeation, and electrostatics: insight into the function of KcsA. *Biochemistry.* 39:13295–13306.

33. Allen, T. W., S. Kuyucak, and S. H. Chung. 1999. Molecular dynamics study of the KcsA potassium channel. *Biophys. J.* 77:2502–2516.

34. Allen, T. W., A. Bliznyuk, A. P. Rendell, S. Kuyucak, and S. H. Chung. 2000. The potassium channel: structure, selectivity and diffusion. *J. Chem. Phys.* 112:8191–8204.

35. Morais-Cabral, J. H., Y. F. Zhou, and R. MacKinnon. 2001. Energetic optimization of ion conduction rate by the K+ selectivity filter. *Nature.* 414:37–42.

36. Berneche, S., and B. Roux. 2001. Energetics of ion conduction through the K+ channel. *Nature.* 414:73–77.

37. Yu, K. Q., W. Fu, H. Liu, X. M. Luo, K. X. Chen, J. P. Ding, and J. H. Shen. 2004. Computational simulations of interactions of scorpion toxins with the voltage-gated potassium ion channel. *Biophys. J.* 86: 3542–3555.

38. DeLano, W. L. 2002. The PyMOL Molecular Graphics System. DeLano Scientific, San Carlos, CA.